In RSS 2013 Workshop on Resource-Efficient Integration of Perception, Control and Navigation for Micro Air Vehicles.

Omnidirectional Obstacle Perception and Collision Avoidance for Micro Aerial Vehicles

Matthias Nieuwenhuisen, David Droeschel, Dirk Holz, and Sven Behnke

***Abstract*— In this paper, we propose a complete micro aerial vehicle platform—including hardware setup and processing pipeline—that is able to perceive obstacles in (almost) all directions in its surrounding. In order to compensate for deficiencies of individual obstacle sensors, we make use of different sensor modalities. Detected obstacles are fused and accumulated in a three-dimensional egocentric obstacle map. For avoiding collisions with detected obstacles, we employ a predictive potential field-based approach to relax the assumption of classic approaches that the vehicle can change its dynamic state instantaneously. We present results in simulation and with the integrated robot.**

I. Introduction

In the context of a larger project on three-dimensional semantic mapping of inaccessible areas and objects, we aim at developing a micro aerial vehicle (MAV) that is able to autonomously navigate in suburban areas, especially in the vicinity of buildings, vegetation, and other possibly dynamic objects. In particular, we focus on fast and reliable perception of obstacles in the vicinity of the MAV.

MAVs have attracted much attention in recent robotics research. The level of autonomy of these robots varies, ranging from basic hovering and position holding [1] over trajectory tracking and waypoint navigation [2] to fully autonomous navigation [3]. Limiting factors for increasing autonomy and complexity of MAVs are limited onboard sensing and processing power.

Particularly important for autonomous operation is the ability to perceive obstacles and avoid collisions. Most of today's MAVs are equipped with ultrasonic sensors and camera systems due to their minimal size and weight. Few systems are equipped with 2D laser range finders (LRF) [4], [5]. Hence, collision avoidance, if considered at all, is often restricted to a two-dimensional LRF measurement plane or the limited field of view of cameras [6].

In general, 3D LRFs are widely accepted for mobile robots due to their accurate distance measurements and their large field of view, but rarely used on lightweight MAVs (cf. [7]) due to their weight and size.

In this paper, we present an integrated MAV with multiple sensing modalities, including a lightweight 3D laser scanner. Furthermore, it is equipped with a high-performance onboard computer to overcome the computational limitations of these platforms.

Autonomous Intelligent Systems Group, Computer Science Institute VI, University of Bonn {nieuwenh, droeschel, holz} at ais.uni-bonn.de, behnke at cs.uni-bonn.de

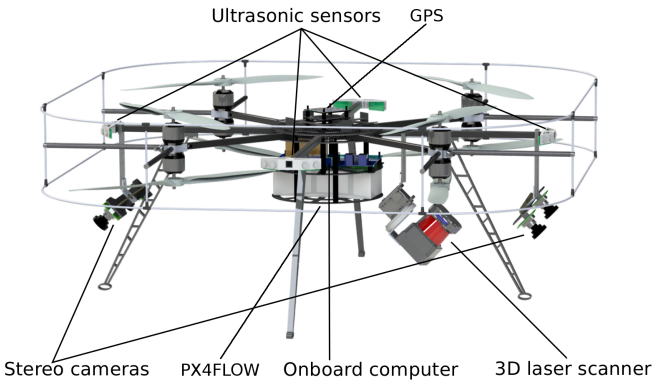

Fig. 1. CAD-model of our MAV with motor arrangement and sensor setup: continuously rotating 3D laser range finder, two stereo camera pairs, an optical flow camera, and a ring of ultrasonic distance sensors.

II. System Setup

We designed our MAV to be compact in order to be able to maneuver in restricted spaces, close to man-made and natural structures. To be able to carry a powerful onboard computer and many sensors (see Fig. 1). We have chosen a design with eight rotors mounted co-axially on four arms that is based on the MikroKopter Octocopter kit. Our MAV has an overall weight of $4.8\,\mathrm{kg}$ and a size of $85\times85\times35\,\mathrm{cm}$. The system is powered by an $8000\,\mathrm{mAh}$ Lithium-Polymer battery pack, yielding a flight time of approximately 10 minutes.

In order to perceive obstacles reliably, we incorporate three different sensor modalities into our system: a 3D laser scanner, stereo camera pairs, and ultrasonic sensors. We have designed a continuously rotating LRF that is minimalistic in terms of size and weight and thus is well suited for operation on MAVs. It is depicted in Fig. 2 and consists of a Hokuyo UTM-30LX-EW 2D LRF which is rotated by a Dynamixel MX-28 servo actuator to create a three-dimensional field of view. This particular Hokuyo LRF is able to measure up to three echoes of a single emitted light pulse. The number of reflected echoes depends on the surface of the object, i.e. shape and reflectivity. For example, transparent material, vegetation or edges of buildings often reflect more than one echo. Hence, multi-echo detection is ideal for outdoor applications. The LRF is electrically connected by a slip ring, allowing for continuous rotation of the sensor. The axis of rotation is pitched downward by 45° in forward direction, which allows for a nearly omnidirectional acquisition of scans with a conical blind spot located upwards behind

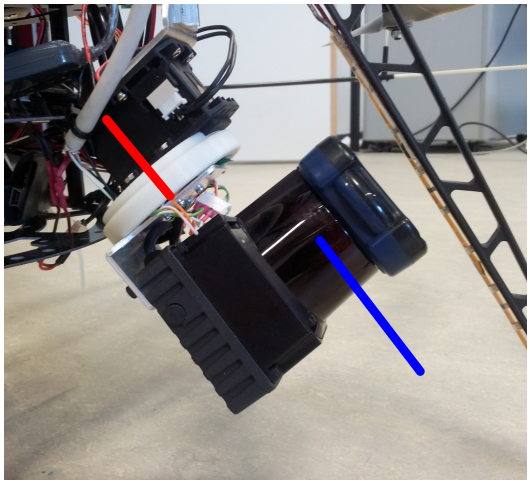

Fig. 2. Our MAV is equipped with an lightweight 3D laser scanner. Point clouds can be acquired at a rate of 2 Hz. The red line depicts the rotation axis and the blue line depicts the measurement plane.

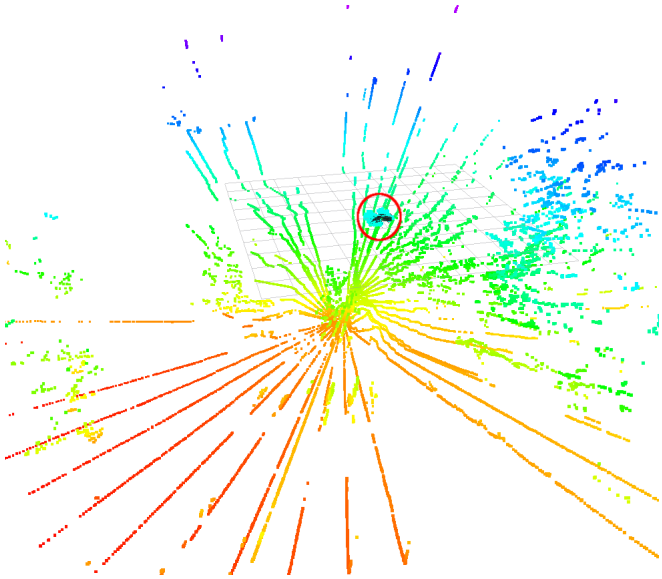

Fig. 3. Example of an acquired 3D laser scan with points color-coded by height. The MAV (circled) is flying in a height of approx. 7.5 m and measures points on the ground as well as buildings and trees surrounding it.

the MAV. A half rotation leads to a full 3D scan of the environment with 21,600 points at a rate of 2 Hz. A typical 3D laser scan acquired during flight is shown in Fig. 3.

In addition to the almost omnidirectional 3D laser scanner, the MAV is equipped with two stereo camera pairs for visual obstacle detection. Both camera pairs are slightly tilted downwards and allow for seeing both ground and environmental structures below and around the MAV. One camera pair is mounted forwards, the other backwards. All four cameras have fisheye lenses with an apex angle up to 185° providing a large field of view.

Neither the laser point cloud nor the visual obstacle detection can perceive very small or transparent obstacles reliably. In order to compensate for this shortcoming and cover these cases, our MAV is equipped with additional eight ultrasonic sensors covering the near space around the MAV.

This sensor setup allows the MAV to perceive obstacles almost omnidirectionally. All sensor information is processed onboard in real-time on an Intel Core i7 quad-core processor with 8 GB RAM. In order to retrieve higher-level mission plans and exchange information with advanced components on a base station computer, we use a WIFI link. With a maximum output power of 2 W it allows for a reliable communication even over long distances.

III. Sensor Processing

Due to the large field of view of the laser range scanner, a considerable amount of points is either measured directly on the robot itself, or caused by occlusion effects. We filter such measurements by checking the robot-centric point coordinates against a simplified model of our robot.

After filtering out self measurements, we use the acquired 3D laser scans to obtain an accurate height estimate. We first compute the set of points below the robot and then find the most dominant (nearly) horizontal plane for these points. We use the distance of the robot to the estimated ground plane as a height estimate. In addition, we can distinguish the ground from other obstacles around the MAV.

The distance measurements outside the MAV are accumulated in an egocentric 3D grid-based map which is centered around the robot. For each distance measurement the corresponding map cell is marked as occupied.

Along with the occupancy information, each cell also maintains its 3D scan points. These 3D points can be used for point-based scan processing, for example 3D scan registration.

We aim for efficient map management for translation and rotation. To this end, individual grid cells are stored in a circular buffer to allow shifting of elements in constant time. We interlace multiple circular buffers to obtain a map with three dimensions. The length of the circular buffers depends on resolution and size of the map. In case of a translation of the MAV, the circular buffers are shifted whenever necessary to maintain the egocentric property of the map.

Since rotating the map would necessitate to shuffle all cells, our map is oriented independently of the MAV's orientation. We maintain the orientation between the map and the MAV and use it to rotate measurements when accessing the map.

Our visual obstacle detection is based on KLT feature tracks matched between the two video streams of one stereo pair. These matched tracks yield 3D points on objects that are not necessarily visible in the LRF measurements at a higher rate than the LRF.

IV. State Estimation and Control

To control the MAV, we need an accurate estimate of the dynamic state of the MAV at a rate equal or higher than the control frequency. The plurality of installed sensors provides us with measurements of subsets of the state variables.

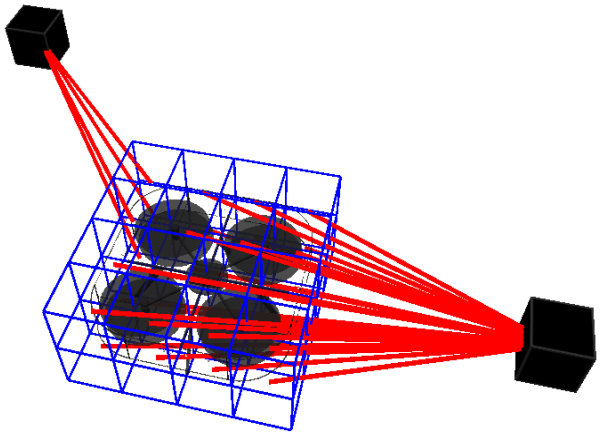

Fig. 4. Artificial forces (red) estimated by our potential field-based approach to collision avoidance are applied to different parts of the MAVs bounding volume (blue). Obstacles do not need to be enlarged by the radius of the volume and multiple obstacles can contribute to the repulsive force.

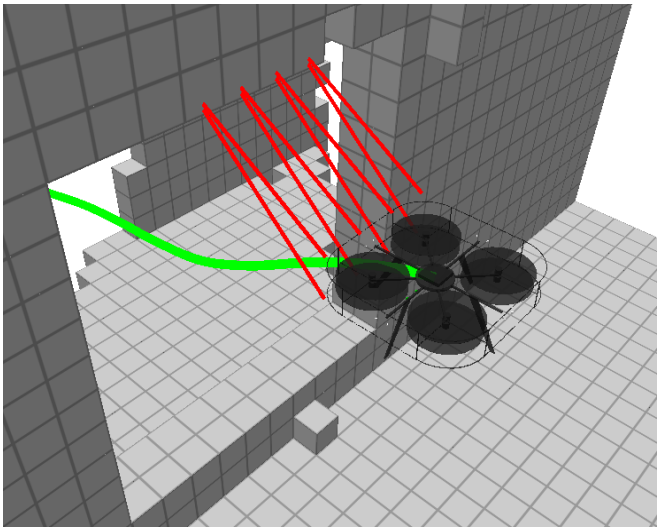

Fig. 5. We predict the influence of a motion command by rolling out the robot's trajectory (green) using a motion model. The current artificial repulsive forces are depicted in red.

Furthermore, not every sensing modality is available in every situation. We fuse these measurements to a single state estimate using an extended Kalman Filter (EKF) based on the Bayesian Filtering Library [8].

Up to a height of 5 m we incorporate velocity measurements from an optical flow camera [9] at 100 Hz. Other means of velocity measurements are visual odometry using our fisheye cameras with PTAM [10] at approximately 20 Hz and GPS velocity measurements at 5 Hz coming from an u-blox LEA-6S GPS chip. This sensor is also the only source of absolute position information, if needed.

The main source for height measurements is the barometric sensor on the MikroKopter FlightControl board. In the initialization routine of the MAV, the sensor is calibrated and initialized to zero height. This sensor works under all conditions and at a high rate, but is subject to drift over time. Thus, it is mainly a good source of relative height changes. We correct these measurements with ultrasonic height measurements within the operational range of the PX4FLOW camera and with laser range measurements at 2 Hz up to a height of 30 m. The attitude of the MAV is estimated using the inertial measurement unit (IMU) on the FlightControl board.

Low-level attitude control of the MAV is performed by the FlightControl board using gyroscope and accelerometer measurements from its onboard IMU. Commands are in the form $(roll, pitch, v_{yaw}, throttle)$. To control the velocity of the MAV, we employ PID controllers on the onboard computer. Input to these controllers are the state estimate from the EKF and a target velocity $v = (v_x, v_y, v_z, v_{yaw})$. The control outputs are sent to the FlightControl board via a serial link at a rate of 20 Hz.

V. Local Obstacle Avoidance

Our concept for the navigation of the MAV is based on a multi-layer approach. Between low-level control and high-level planning layers, we employ a fast reactive collision avoidance module based on artificial potential fields [11]. This enables the MAV to immediately react to nearby obstacles and deviations from a planned path.

In contrast to the standard potential field-based approach, we relax the assumption that the robot is an idealized particle. We account for the shape of the MAV by discretizing it into cells of the size of our 3D grid map (see Fig. 4). The center points of these cells are individual particles to the algorithm. Hence, obstacles induce repulsive forces and the target waypoint induces an attractive force on each of these cells. Thus, multiple obstacles can induce forces on different parts of the MAV. The resulting force to the MAV is now the average of the weighted sums of the individual attractive and repulsive forces.

Standard potential field approaches assume that the motion of a vehicle can be changed immediately. To overcome this limitation, we predict the MAV's future trajectory T_t given the current dynamic state x_t and the probable sequence of motion commands $u_{t:t+n}$ for a fixed discrete-time horizon n (Fig. 5). This time horizon is tightly bound by the property that multicopters can quickly stop or change their motion. To predict the trajectory, we employ a motion model of the MAV and the estimated resulting forces along the trajectory. The magnitudes of the velocity commands are calculated according to the predicted future forces.

We model the MAV as linear dynamic system with state transition matrices A and B. The prediction of the future trajectory for the next n time steps is then given by

$$\begin{aligned} T_t &= p_{t:t+n} = (p_t, p_t + 1, \ldots, p_{t+n}), \\ p_{i+1} &= Ax_i + Bu_i + p_i \qquad i \in [t : t + n - 1], \\ u_i &= C\vec{F_{p_i}}. \end{aligned}$$

The future control commands u_i are predicted by mapping the estimated forces $\vec{F_{p_i}}$ at a position p_i to a control command with matrix C. If a given force threshold is exceeded

TABLE I

EFFECT OF SLOWING DOWN WITH 1 S TRAJECTORY LOOK-AHEAD COMPARED TO THE STANDARD POTENTIAL FIELD APPROACH (PF).

	Time (s)	Avg. Force	Frac. of PF
PF	11.9 (0.5)	0.44 (0.06)	1
Adaptive Vel. 1 s	12.9 (0.8)	0.3 (0.01)	0.68

at any point p_i of the trajectory, we reduce the velocity v of the MAV to

$$v_{new} = \left(\frac{1}{2} + \frac{i}{2n}\right) v_{max}.$$

We can learn a motion model (time-discrete linear dynamic system) by flying with a MAV within our motion capture system. In addition to predicting the trajectory for the purpose of collision avoidance, this model can be utilized in low-level velocity controllers [12] and for kinodynamic motion planning [13]. Furthermore, we use it in our Gazebo-based simulation environment (cf. [14]) to ensure realistic behavior of the simulated multicopter.

In addition to guiding the MAV collision free to waypoints, our approach can act as a safety copilot to assist a human pilot. As the human pilot sends direct motion commands instead of coordinates relative to the MAV, we omit the attractive force in this case. Instead, we directly influence the control command given by the pilot if the MAV operates in the vicinity of obstacles. Repulsive forces induce a delta command that is added to the original control command, yielding a stop or deviation from the commanded direction.

VI. EXPERIMENTS

We evaluated the effect of slowing down the MAV according to predicted future artificial forces in simulation. In a waypoint following scenario through walls with windows of different size the average repulsive force applied to the MAV using the predictive potential field approach were 68% of the force occurring during the flights without trajectory prediction. The average flight time was slightly increased from 11.9 s to 12.9 s. Tab. I summarizes the results. Overall, the resulting trajectories are smoother as the MAV is not repulsed so much from obstacles, especially between parallel walls. Experiments on the integrated robot up to now have shown that the hovering octocopter can perceive and avoid approaching obstacles. We also tested the proposed safety layer successfully on our MAV. It stayed away from static obstacles while flying remote controlled.

VII. CONCLUSIONS

We presented a MAV equipped with a multi-modal sensor setup for robust obstacle detection using ultrasonic sensors, fisheye stereo cameras and a lightweight 3D LRF. Based upon this setup, we developed a fast, reactive collision avoidance layer to quickly react on new measurements of nearby obstacles. Experiments in simulation revealed that our predictive collision avoidance leads to smoother trajectories, keeping the MAV further away from obstacles than a classic potential field approach without prediction. The simulated MAV was able to fly through passageways of its size plus a safety margin.

In future work we will extend our control architecture with high-level planning layers to avoid obstacles on a coarser time-scale and to accomplish more complex mission goals.

ACKNOWLEDGMENTS

This work has been supported by grant BE 2556/7,8 of German Research Foundation (DFG).

REFERENCES

[1] S. Bouabdallah, P. Murrieri, and R. Siegwart, "Design and control of an indoor micro quadrotor," in *Proceedings of the IEEE International Conference on Robotics and Automation (ICRA)*, 2004.

[2] T. Puls, M. Kemper, R. Kuke, and A. Hein, "GPS-based position control and waypoint navigation system for quadrocopters," in *Proceedings of the IEEE/RSJ International Conference on Intelligent Robots and Systems (IROS)*, 2009.

[3] S. Grzonka, G. Grisetti, and W. Burgard, "A fully autonomous indoor quadrotor," *IEEE Transactions on Robotics*, vol. 28, no. 1, pp. 90–100, 2012.

[4] T. Tomić, K. Schmid, P. Lutz, A. Domel, M. Kassecker, E. Mair, I. Grixa, F. Ruess, M. Suppa, and D. Burschka, "Toward a fully autonomous UAV: Research platform for indoor and outdoor urban search and rescue," *IEEE Robotics Automation Magazine*, vol. 19, no. 3, pp. 46–56, 2012.

[5] S. Grzonka, G. Grisetti, and W. Burgard, "Towards a navigation system for autonomous indoor flying," in *Proceedings of the IEEE International Conference on Robotics and Automation (ICRA)*, 2009.

[6] T. Mori and S. Scherer, "First results in detecting and avoiding frontal obstacles from a monocular camera for micro unmanned aerial vehicles," in *Proceedings of the IEEE International Conference on Robotics and Automation (ICRA)*, 2013.

[7] A. Chambers, S. Achar, S. Nuske, J. Rehder, B. Kitt, L. Chamberlain, J. Haines, S. Scherer, , and S. Singh, "Perception for a river mapping robot," in *Proceedings of the IEEE/RSJ International Conference on Intelligent Robots and Systems (IROS)*, 2011.

[8] K. Gadeyne, "BFL: Bayesian Filtering Library," http://www.orocos.org/bfl, 2001.

[9] D. Honegger, L. Meier, P. Tanskanen, and M. Pollefeys, "An open source and open hardware embedded metric optical flow cmos camera for indoor and outdoor applications," in *Proceedings of the IEEE International Conference on Robotics and Automation (ICRA)*, 2013.

[10] G. Klein and D. Murray, "Parallel tracking and mapping for small AR workspaces," in *Proceedings of the sixth IEEE and ACM International Symposium on Mixed and Augmented Reality (ISMAR)*, 2007.

[11] S. Ge and Y. Cui, "Dynamic motion planning for mobile robots using potential field method," *Autonomous Robots*, vol. 13, no. 3, pp. 207–222, 2002.

[12] M. Achtelik, A. Bachrach, R. He, S. Prentice, and N. Roy, "Autonomous navigation and exploration of a quadrotor helicopter in GPS-denied indoor environments," in *Proceedings of the IEEE International Conference on Robotics and Automation (ICRA)*, 2009.

[13] I. Şucan and L. Kavraki, "Kinodynamic motion planning by interior-exterior cell exploration," *Algorithmic Foundation of Robotics VIII*, pp. 449–464, 2009.

[14] N. Koenig and A. Howard, "Design and use paradigms for Gazebo, an open-source multi-robot simulator," in *Proceedings of the IEEE/RSJ International Conference on Intelligent Robots and Systems (IROS)*, 2004.